

# A method of estimating the Martian neutral atmospheric density at 130 km, and comparison of its results with Mars Global Surveyor and Mars Odyssey aerobraking observations based on the Mars Climate Database outputs

JunFeng Qin<sup>1</sup>, Hong Zou<sup>1\*</sup>, YuGuang Ye<sup>1</sup>, YongQiang Hao<sup>1</sup>, JinSong Wang<sup>2</sup>, and Erling Nielsen<sup>3</sup>

<sup>1</sup>Institute of Space Physics and Applied Technology, School of Earth and Space Science, Peking University, Beijing 100871, China;

<sup>2</sup>National Center for Space Weather, China Meteorological Administration, Beijing 100081, China;

<sup>3</sup>Max Planck Institute for Solar System Research, Katlenburg-Lindau 37191, Germany

## Key Points:

- The neutral densities at 130 km in the Martian northern high latitudes were calculated by using the ionospheric profiles observed by Mars Global Surveyor (MGS) radio occultation observations
- A technique for modifying Mars Climate Database (MCD) v4.3 outputs was found based on the calculated neutral densities at 130 km
- The MGS and Mars Odyssey (ODY) aerobraking-observed neutral densities at 130 km were compared with MCD v4.3 outputs to verify the method used to calculate the neutral densities at 130 km and the technique used to modify the MCD v4.3 outputs

**Citation:** Qin, J. F., Zou, H., Ye, Y. G., Hao, Y. Q., Wang, J. S., and Nielsen, E. (2020). A method of estimating the Martian neutral atmospheric density at 130 km, and comparison of its results with Mars Global Surveyor and Mars Odyssey aerobraking observations based on the Mars Climate Database outputs. *Earth Planet. Phys.*, 4(4), 408–419. <http://doi.org/10.26464/epp2020038>

**Abstract:** Profiles of the Martian dayside ionosphere can be used to derive the neutral atmospheric densities at 130 km, which can also be obtained from the Mars Climate Database (MCD) and spacecraft aerobraking observations. In this research, we explain the method used to calculate neutral densities at 130 km via ionosphere observations and three long-period 130-km neutral density data sets at northern high latitudes (latitudes  $> 60^\circ$ ) acquired through ionospheric data measured by the Mars Global Surveyor (MGS) Radio Occultation Experiment. The calculated 130-km neutral density data, along with 130-km density data from the aerobraking observations of the MGS and Mars Odyssey (ODY) in the northern high latitudes, were compared with MCD outputs at the same latitude, longitude, altitude, solar latitude, and local time. The 130-km density data derived from both the ionospheric profiles and aerobraking observations were found to show seasonal variations similar to those in the MCD data. With a negative shift of about  $2 \times 10^{10} \text{ cm}^{-3}$ , the corrected 130-km neutral densities derived from MCD v4.3 were consistent with those obtained from the two different observations. This result means that (1) the method used to derive the 130-km neutral densities with ionospheric profiles was effective, (2) the MCD v4.3 data sets generally overestimated the 130-km neutral densities at high latitudes, and (3) the neutral density observations from the MGS Radio Science Experiment could be used to calibrate a new atmospheric model of Mars.

**Keywords:** Martian upper atmosphere; Mars Climate Database v4.3; aerobraking observations; Mars global circulation

## 1. Introduction

Early in the 1780s, Mars was found to have an atmosphere, based on periodic changes in the area of the Martian polar crest and terrestrial observations of the edge of Mars (Herschel, 1784). This was the beginning of Martian atmospheric research. When Mariner 4 flew by Mars in 1965, the Martian atmosphere and ionosphere were observed for the first time via radio occultation, and through this method, the first profile of the Martian ionosphere was de-

rived (Fjeldbo et al., 1966). With knowledge of the basic parameters of the Martian atmosphere, some single-circle circulation models were developed to characterize the Martian global circulation (Zurek, 2017). In 1971, Mariner 9 became the first orbiter to make long-term observations of the Martian atmosphere, followed by two Viking probes and their landers. The atmospheric observations made by Mariner 9 and Viking 1 and 2 greatly improved research on the composition of the Martian atmosphere and its seasonal changes, CO<sub>2</sub> circulation, H<sub>2</sub>O circulation, dust storms, and global atmospheric circulation patterns (Nier and McElroy, 1976; Jakosky and Farmer, 1982; Ryan, 1985; Clancy and Lee, 1991). On the basis of these data and research studies, classical Martian atmosphere circulation models (represented by the Laboratoire de Météorologie Dynamique Mars Global Circulation Model (LMD-

Correspondence to: H. Zou, hongzou@pku.edu.cn

Received 11 FEB 2020; Accepted 10 APR 2020.

Accepted article online 09 JUN 2020.

©2020 by Earth and Planetary Physics.

MGCM) and Mars Thermospheric General Circulation Model (MT-GCM)) were considerably improved and became reliable. As the 20th century transitioned to the 21<sup>st</sup> century, the Mars Pathfinder, Mars Global Surveyor (MGS), Mars Odyssey (ODY), Mars Express (MEX), Mars Reconnaissance Orbiter, and Mars Science Laboratory were successively launched to Mars. Observations from these orbiters, landers, and rovers gave researchers a global, systematic, and refined understanding of the Martian atmosphere. With these detailed and plentiful data, the scope and accuracy of Martian global atmospheric circulation models were further improved. At present, models such as the Mars General Circulation Model–Mars Thermosphere General Circulation Model (MGCM-MT-GCM) and the Mars Global Ionosphere–Thermosphere Model (M-GITM) have been able to simulate the Martian atmosphere from the surface to the thermosphere (González-Galindo et al., 2006; Bougher et al., 2015). As can be seen from the history of Martian atmospheric research and Martian atmospheric modeling research, the development and improvement of Martian atmospheric models relies heavily on the support of long-term, wide-ranging, and high-quality observation data.

Currently, the main methods of detecting the Martian neutral atmosphere include aerobraking, in situ, spectrometer, and radio occultation observations. The density data derived from aerobraking measurements onboard the MGS and ODY have aided research exploring gravity waves, nonmigrating waves, and instability in the Martian upper atmosphere (Bougher et al., 2001; Wilson, 2002; Fritts et al., 2006). In the recent Mars Atmosphere and Volatile Evolution (MAVEN) mission, aerobraking measurements and Neutral Gas and Ion Mass Spectrometer (NGIMS) in situ observations captured the neutral density of different species at a height as low as 135 km during the deep-dip phases (Dong et al., 2015; Mahaffy et al., 2015). Limited by the orbit design, the aerobraking and in situ observations have so far been able to derive density data only at an altitude higher than 100 km, and long-term high-latitude observations are still rare (Keating et al., 1998, 2003, 2007). The Spectroscopy for Investigation of Characteristics of the Atmosphere of Mars (SPICAM) onboard MEX and the Imaging Ultraviolet Spectrograph (IUVS) onboard MAVEN have respectively observed Martian atmospheric pressure and temperature profiles at 60–130 km and 100–150 km through stellar occultation (Forget et al., 2009; Gröller et al., 2015). These spectrometer observations have been very useful in research on the upper atmosphere, but the coverage of this observation is still poor at local times and in local seasons. Apart from IUVS/MAVEN and SPICAM/MEX, the Thermal Emission Spectrometer (TES) on the MGS and the Mars climate sounder on the Mars Reconnaissance Orbiter can also use spectrometer observations to derive temperature profiles and dust, water ice, and dry ice profiles in the lower and middle atmosphere, and these data have played an important role in the study of Martian climate evolution (Kleinböhl et al., 2009). In addition, radio occultation observations, as an effective and inexpensive technique for acquiring the atmospheric neutral density, have been widely used in almost all the Mars probes. However, only the neutral densities of the lower and middle atmosphere can be derived from radio occultation observations. For example, in the MGS radio occultation experiment, only the neutral density data at 0–50 km were reliable (Hinson et al., 2004), although radio oc-

ultation measurements are an important means of studying the planetary ionosphere. It can be concluded, based on the above discussions, that to date, long-term observations of the Martian upper atmospheric densities in high-latitude regions are still rare.

Without a strong magnetic field, particles from the solar wind would interact directly with the Martian atmosphere and cause instability and loss of the upper atmosphere. At the same time, variation in the solar radiation could easily change the thermal structure of the upper atmosphere (Jain et al., 2016). Furthermore, the waves and activities of the lower atmosphere (e.g., gravity waves, dust storms, etc.) could affect the structure of the Martian upper atmosphere and ionosphere (Withers and Pratt, 2013; Qin JF et al., 2019a). For these reasons, the upper atmosphere of Mars is quite unstable and unpredictable. Hence, at present, the classic models of the Martian atmosphere are still problematic in their simulations and prediction of the upper atmospheric densities. Moreover, a phenomenon exists in which the Martian pole areas might be heated by the adiabatically sinking airflow, which is controlled by global circulation (Lewis et al., 2007; Medvedev et al., 2013), and this mechanism makes the density of the high-latitude upper atmosphere more difficult to simulate and predict.

As explained above, Martian atmospheric circulation models do not perform well in the region of the high-latitude upper atmosphere, and long-term observations of this region are not rich enough to support research on and simulations of the upper atmosphere. Thus, the study and modeling of the Martian upper atmosphere are of great importance to current and future Mars projects, given that fluctuations in the upper atmosphere can significantly affect low-orbit detectors and aerobraking landers and that the ionosphere embedded in the middle and upper atmosphere can affect communication between the landers and orbiters. For this situation, the coupling between the Martian neutral atmosphere and ionosphere was researched and a method was proposed to calculate Martian neutral densities at 130 km (the average altitude of the main peak height of the Martian ionosphere) through ionospheric profiles (Zou H et al., 2005, 2006, 2011). With this method, three long-period ionospheric observations from the MGS radio occultation experiment were used to estimate the neutral densities at 130 km in the northern high-latitude regions (Zou H et al., 2016). In this research, we compared the calculated densities with the outputs of the Mars Climate Database (MCD, which is based on the LMD-MGCM) and then found a way to modify the outputs of MCD v4.3.

To verify the method used by Zou H et al. (2016) to calculate 130-km neutral densities by using ionospheric profiles and their technique for modifying MCD v4.3, in this research, we compared two other relatively short-term measurements of 130-km neutral densities — those made by the MGS and ODY aerobraking observations in the northern high latitudes — with the unmodified versus modified MCD v4.3 outputs. The seasonal coverage of aerobraking data is at 260°–300° solar latitude ( $L_s$ ), whereas the coverage of the MGS radio occultation measurements is at  $L_s$  70°–230°. In this way, we could further determine whether the technique for modifying MCD v4.3 could be used in the dust storm season ( $L_s$  180°–360°), during which Martian global dust storms frequently appear and the upper atmosphere becomes more unstable at

high latitudes. Moreover, by comparing the trends of aerobraking data with the MCD outputs, we were able to obtain useful information on the LMD-MGCM simulation of the high-latitude upper atmosphere during global dust storms.

The data and atmospheric model used in this research are introduced in Section 2, and the method used to derive neutral densities at 130 km from ionospheric profiles is explained in Section 3. The main results comparing the aerobraking data with the MCD outputs are shown in Section 4, followed by a discussion in Section 5 and the conclusions in Section 6.

## 2. Data and the Model

### 2.1 MGS Radio Occultation Data

The ionospheric profiles used to derive neutral densities at 130 km were from radio occultation observations made by the MGS during November 2000–July 2001, November 2002–July 2003, and November 2004–July 2005 (corresponding to Ls 65°–175° in Martian year [MY] 25, Ls 85°–200° in MY26, and Ls 120–230° in MY27). All these data could be found in the Planetary Data System. According to Hinson et al. (1999), MGS radio occultation measurements can acquire an electron density higher than  $10^3/\text{cm}^3$  at 80–200 km, meaning that the main peak height profiles of the Martian ionosphere could be measured precisely.

Depending on the period of the MGS orbit and the geometric relationship between Mars and the Earth, 8–12 profiles of the ionosphere with similar latitudes, solar longitudes, solar zenith angles (SZAs), local times, and discrete longitudes could be observed

each day. Figure 1 shows the main parameters of the ionospheric profiles (peak altitudes and scale heights at the peak altitudes) and observational geometric (SZAs, local times, longitudes, and latitudes) of the three data sets. Note that all these observations were made in the northern high latitudes (60°–90°N), with the continuous local time, SZA, latitude, and evenly dispersed longitude varying with Ls.

### 2.2 MGS and ODY Aerobraking Data

Mars Global Surveyor aerobraking observations began in September 1997 and ended in March 1999. During this operation, the orbit duration of the orbiter diminished from about 45 hours to about 2 hours. According to Tolson et al. (1999), each of the accelerometers onboard MGS was able to measure a velocity variation of at least 0.332 mm/s, providing a sensitivity 38 times higher than those of the Viking probes. At this sensitivity, the neutral density data derived from the MGS aerobraking observations had an accuracy of 3% (below 140 km). In the Planetary Data System, both 7-s-averaged density data and 40-s-averaged density data are provided, but only the former were used in this research.

Because we focused on the neutral density at 130 km in the northern high-latitude regions in this study, only the relatively long-term aerobraking observations made at the northern high latitudes were adopted. These kinds of observations were made by the MGS at Ls 282°–299° in MY23, as shown in Figure 2. During that period, the perigee height of the MGS orbits stayed as high as 120 km, meaning that the inbound and outbound observations shared similar latitudes, longitudes, local times, and SZAs (see Figure 2).

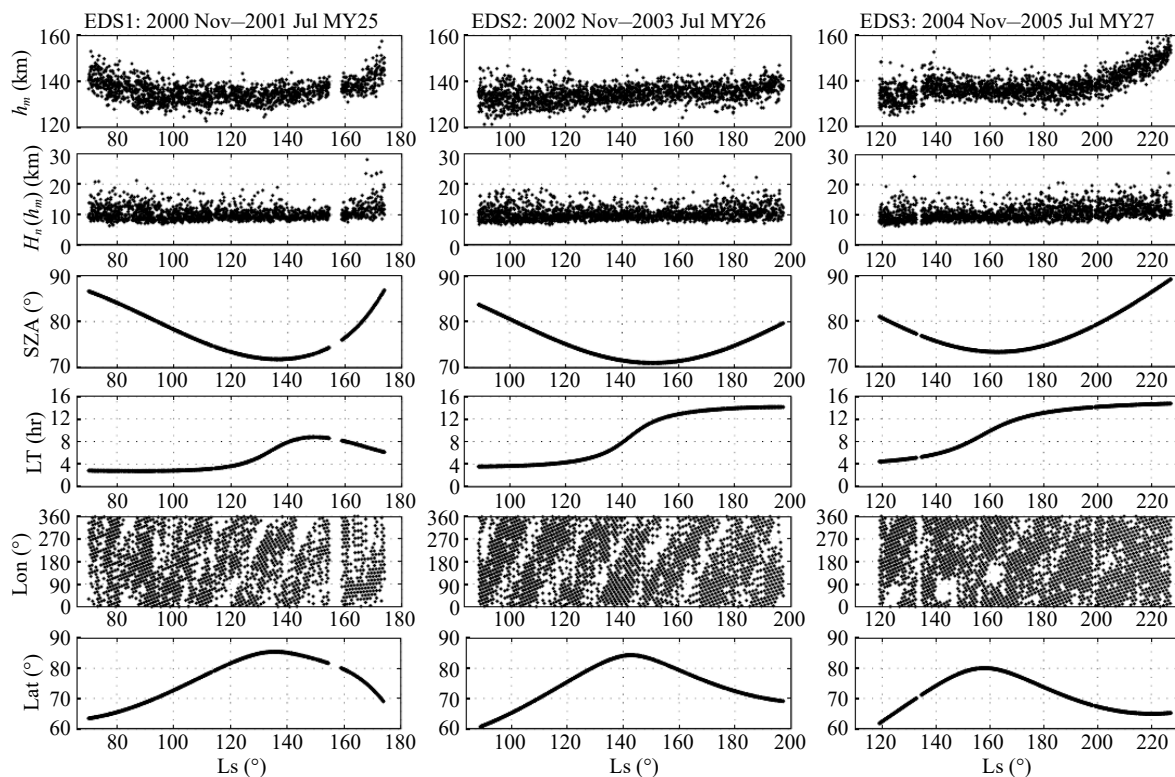
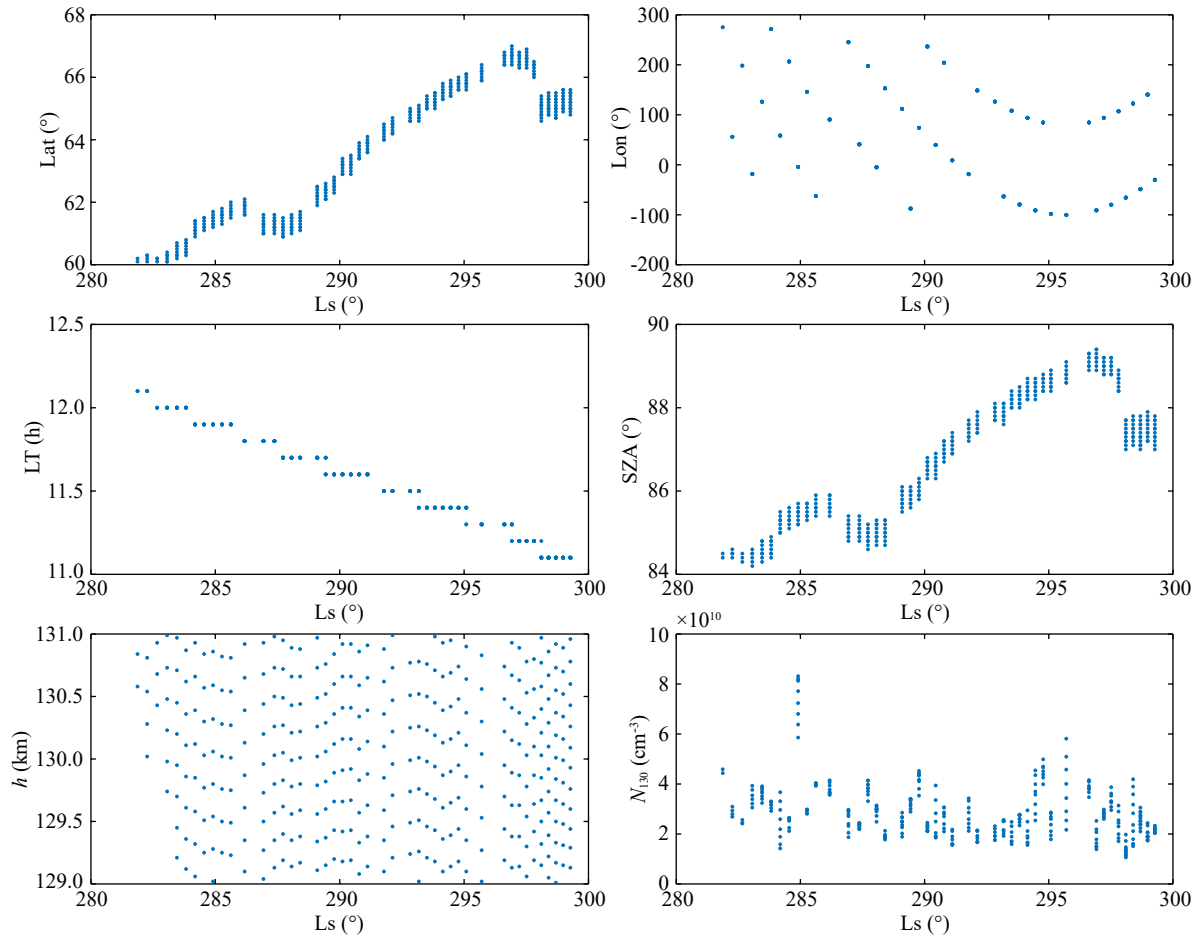


Figure 1. Main parameters of the MGS radio occultation observations (Zou H et al., 2016).



**Figure 2.** Main parameters of the MGS aerobraking observations.

The ODY aerobraking observations began in October 2001 and ended in January 2002. During the operation, the orbit duration of the orbiter diminished from about 18 hours to about 2 hours. According to Tolson et al. (2005), because of a change in the sampling rate of the accelerometers during the mission, the uncertainty varied from 0.07 to 0.5 mm/s<sup>2</sup> in 1-s count times, equivalent to a neutral density uncertainty of 0.15 to 1.1 kg/m<sup>3</sup> (thus a number density uncertainty of 0.2 to 1.5 × 10<sup>10</sup>/cm<sup>3</sup>). The density data adopted in this research had an uncertainty of less than 10<sup>10</sup>/cm<sup>3</sup>.

Mars Odyssey aerobraking was measured at northern-latitude neutral densities of 130 km at Ls 263°–304° in MY25 (see Figure 3). What must be emphasized is that the perigee height of the ODY orbits remained lower than 100 km during this period, causing the inbound and outbound observations to have very different latitudes, local times, and SZAs (see Figure 3). Another consequence of such a low perigee is that with the potential effect of a rise in temperature (which happened in every aerobraking phase) on the accuracy of the accelerometers, inbound and outbound data may have had different systematic errors (Tolson et al., 2005). For the reasons above, the ODY inbound and outbound data series are distinguished in this research.

### 2.3 MCD v4.3

The MCD, a database of Martian climate and environment, is

based on the simulation outputs of LMD-MGCM under different solar radiation conditions and dust scenarios. This database includes Martian atmospheric temperature, pressure, wind field, and neutral density, as well as the mixing ratios of water vapor, water ice, and different neutral components in the region below 250 km (Millour et al., 2008).

After decades of research and optimization, the MCD has been updated to version 5.3. However, when we first attempted to compare MGS Radio Science data with MCD outputs in the work by Zou H et al. (2011), the MCD had been updated only to version 4.3. To maintain consistency in the research, the MCD v4.3 outputs were again adopted in this research. Furthermore, although we attempted to use the latest version of the MCD in this research, the outputs of MCD v5.X showed completely different seasonal variations than those from the MGS observations. This situation is also discussed in Qin JF et al. (2019a, b).

According to Millour et al. (2008), MCD v4.3 is able to provide simulated atmospheric density data under minimum, average, and maximum solar radiation conditions as well as cold, warm, and dust storm dust scenarios for MY24. In this research, the conditions were set to the maximum solar radiation conditions and the dust storm scenario of MY24, for consistency with Zou H et al. (2016).

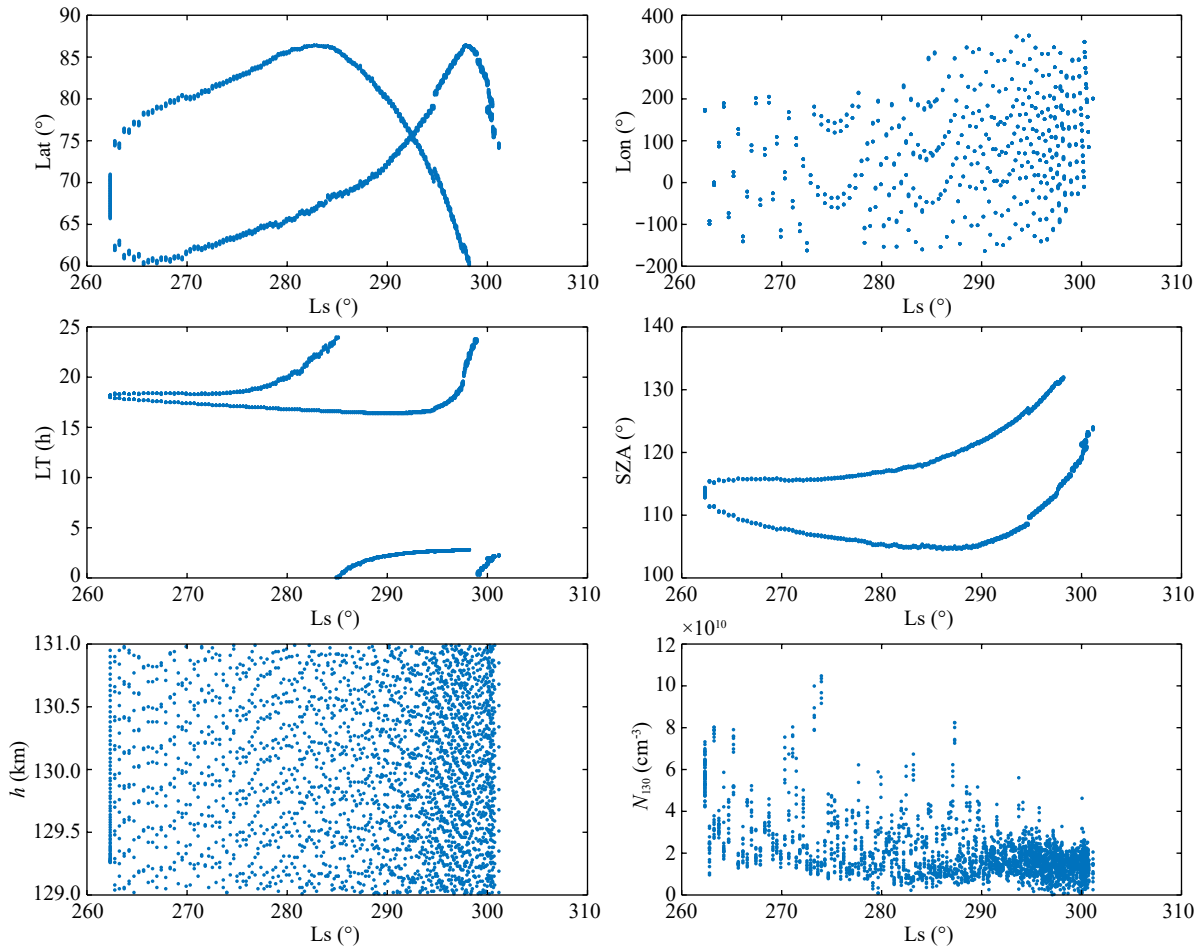


Figure 3. Main parameters of the ODY aerobraking observations.

3. Method of Calculating Neutral Densities at 130 km

According to Chapman theory, the maximum electron density of a planetary ionosphere is thought to happen in the atmospheric level where  $\tau = 1$ , that is, in the case of Mars,

$$\tau = \sigma \cdot \int_{l_0}^{\infty} N_m dl = \sigma \cdot \sec \chi \cdot \int_{h_0}^{\infty} N_m dh = \sigma \cdot \sec \chi \cdot N_m(h_m) \cdot H_n(h_m) = 1, \quad (1)$$

where  $\sigma$  represents the mean cross section of  $\text{CO}_2$ ,  $\chi$  represents the SZA,  $h_m$  represents the ionospheric main peak height,  $N_m$  represents the neutral density,  $l$  represents the path of solar radiation in the atmosphere, and  $H_n$  represents the scale height of the neutral atmosphere.

The consistency between the theory-based Chapman ionosphere and the vicinity of the actual main peak of the Martian ionosphere has been researched at length. Theoretically, the magnitude of the peak electron density for a given solar radiation at a SZA of  $\chi$  is equal to  $n_0(\cos \chi)^b$ , where  $n_0$  is the subsolar maximum electron density and  $b$  is 0.5 for an ideal Chapman ionosphere (i.e., a molecular ion-dominant ionosphere). Zhang et al. (1990), Breus et al. (2004), and Zou H et al. (2006), respectively, calculated the value of  $b$  in the Martian ionosphere by using data from Mariner 9, Viking orbiters, and the MGS, and they all found  $b_{\text{Mars}}$  quite close to 0.5 (0.57 for Zhang et al., 1990, 0.5 for Breus et al., 2004, and 0.44 for Zou H et al., 2006). According to these results, the main peak of the Martian ionosphere is quite close to a Chapman-like

ionosphere, meaning that Equation (1) is effective in the main peak region of the Martian ionosphere.

Further derivations and verification of Equation (1) can be found in Breus et al. (2004). Equation (1) shows the coupling between the neutral atmosphere and the main peak of the ionosphere. Furthermore, according to Breus et al. (2004), the electron density  $n$  near the main peak height of the Martian ionosphere can be approximately described as a quadratic function of height  $h$ :

$$n(h) = a + bh + ch^2, \quad (2)$$

in which  $a = n_m \left(1 - \frac{h_m^2}{4H_n^2}\right)$ ,  $b = \frac{n_m h_m}{2H_n^2}$ ,  $c = -\frac{n_m}{4H_n^2}$ ,  $H_n$  represents the neutral scale height at height  $h$ , and  $n_m$  represents the peak electron density.

On the basis of Equation (2), assuming that the neutral scale height is a constant in the regions near the main peak of the ionosphere, the mean neutral scale height  $H_n$  and peak altitude  $h_m$  can be acquired from the ionospheric profiles. When  $H_n$  is derived and  $\chi$  and  $\sigma$  are defined, according to Equation (1), the neutral density at height  $h_m$  can be calculated, which is

$$N_m \approx \frac{\cos \chi}{\sigma \cdot H_n(h_m)}. \quad (3)$$

Because the main peak height of the Martian ionosphere is

around 130 km, it is acceptable to use the mean scale height  $H_n$  as the scale height between 130 km and  $h_m$ . We then get a 130-km neutral density:

$$N_{130} = N_m \cdot \exp\left(\frac{h_m - 130}{H_n}\right). \quad (4)$$

#### 4. Comparisons Among the Calculated 130-km Density Data, Aerobraking Data, and MCD v4.3 Outputs

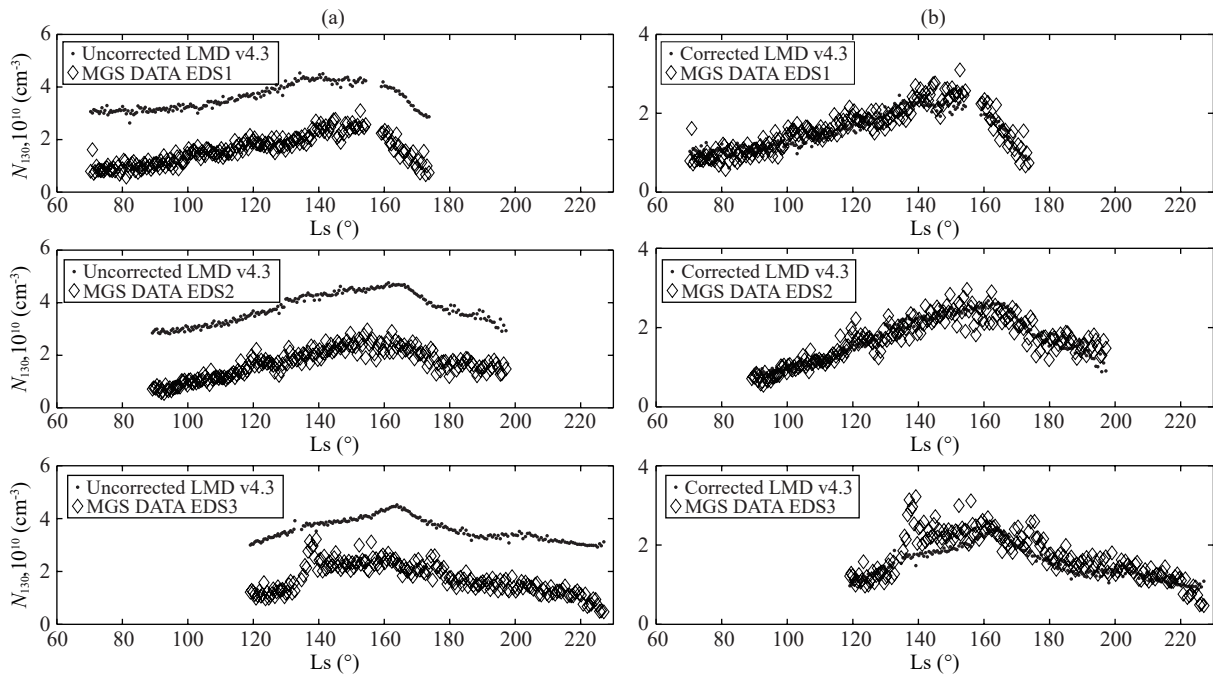
Through the method above, we were able to derive the neutral density at 130 km from the ionospheric profiles observed by the MGS radio occultation measurements. All the parameters needed to calculate neutral densities at 130 km could be acquired through the MGS radio occultation observations, except for the mean cross section of  $\text{CO}_2$ , which was set as  $2.3 \times 10^{17} \text{cm}^2$  in this research, for consistency with previous research (Wang and Nielsen, 2003; Zou H et al., 2005, 2011, 2016). The calculated 130-km neutral density data were then compared with MCD v4.3 130-km neutral density outputs, which shared the same latitude, longitude, Ls, and local time with MGS observations (shown in Figure 1).

Figure 4a displays the comparison between the calculated 130-km neutral densities from the MGS radio occultation measurements and those simulated from MCD v4.3 over three periods (November 2000–July 2001, November 2002–July 2003, and November 2004–July 2005). As can be seen, during all three periods, the calculated 130-km neutral densities and simulated densities shared analogous variations, and the former held the constant lower than the latter. This situation allowed us to modify the MCD v4.3 outputs through a simple linear function,

$$N_{130\_corrected\_MCD} = AN_{130\_uncorrected\_MCD} + B,$$

for consistency with the observations. By conducting a linear regression on the calculated 130-km neutral densities and MCD outputs in November 2000–July 2001, we could solve that  $A = 0.97 \pm 0.05$  and  $B = (-1.94 \pm 0.25) \times 10^{10} \text{cm}^{-3}$  (Zou H et al., 2016), nearly equivalent to a negative shift of about  $2 \times 10^{10} \text{cm}^{-3}$ . In total, 209 samples were used in the linear regression, and the  $p$ -values of  $A$  and  $B$  were much lower than 0.05. As discussed by Zou H et al. (2016), the coefficients  $A$  and  $B$  were evidently dependent on the value of the mean cross section of  $\text{CO}_2$ . When the value was set as  $2.3 \times 10^{17} \text{cm}^2$ ,  $A$  was close to 1, and  $B$  was close to  $-2 \times 10^{10} \text{cm}^{-3}$ . An increase in the  $\text{CO}_2$  mean cross section could cause a decrease in  $A$  and an increase in  $B$ . Figure 4b shows a comparison between the calculated 130-km neutral densities and the corrected MCD v4.3 outputs. Note that the results of the modified MCD v4.3 outputs were in good agreement with the calculated 130-km neutral densities in three periods, except for Ls  $135^\circ$ – $145^\circ$  MY27, when a local dust storm was occurring at low latitudes and the 130-km neutral densities were uplifted (Qin JF et al., 2019a). This result also showed that the 130-km neutral densities were not sensitive to the solar radiation conditions. The correlation coefficients between the calculated 130-km neutral densities and the MCD outputs shown in Figure 4 were, respectively, 0.886, 0.909, and 0.817 for the data from November 2000–July 2001, November 2002–July 2003, and November 2004–July 2005. Modification of the MCD outputs did not change the correlation coefficients.

The three MGS radio occultation observations of the Martian northern hemisphere at high latitudes were mainly concentrated in the no-dust-storm season (Ls  $< 180^\circ$ ) when there were few global dust storms. To verify the method of calculating the 130-km neutral densities and of modifying the MCD v4.3 outputs, we further compared the 130-km neutral density data observed by MGS



**Figure 4.** (a) Calculated 130-km neutral densities derived from the MGS radio occultation observations in MY25–27 (diamonds) and uncorrected MCD v4.3 outputs (dots); (b) calculated 130-km neutral densities derived from the MGS radio occultation observations in MY25–27 (diamonds) and corrected MCD v4.3 outputs (dots).

and ODY aerobraking measurements during the dust storm season with both the unmodified and modified results from MCD v4.3.

As mentioned in Section 2, MGS aerobraking registered 130-km neutral densities of the Martian northern high latitudes at Ls 282°–299° (MY23), which belongs to a dust storm season. Figure 5 shows MGS aerobraking observations and MCD v4.3 outputs for neutral densities at 130 km. The MGS aerobraking data were 5-point running averaged. As shown in Figure 5, the neutral atmospheric density at 130 km observed by MGS aerobraking showed a typical periodic fluctuation. This fluctuation was also reflected in the outputs from MCD v4.3. As shown in Figure 2, the latitude, local time, and SZA changed only moderately, but the longitude changed violently and periodically during the MGS aerobraking observations, so the fluctuations are thought to be the effect of longitudinal variations. This effect of longitudinal variations on the upper atmosphere of Mars is discussed in detail in the work of Keating et al. (1998), which is also based on observations of MGS aerobraking. In addition, some sudden increases (called “bursts”) in the neutral density at 130 km were observed by MGS aerobraking, such as those near Ls 285°, 295°, and 296°. These sudden increases in observed neutral densities may have been caused by local or short-term dust storms. Because the outputs of the MCD v4.3 are based on dust storm scenarios in MY24, this dust storm caused increases in the neutral densities at 130 km in MY23 that did not appear in the MCD results. As shown in Figure 5, the modified MCD outputs were basically consistent with the MGS aerobraking observations, except for some diversity caused by the different dust scenarios, meaning that the method of modifying the MCD v4.3 outputs was still effective during the dust storm season at Ls 280°–300°. The correlation coefficient between the densities observed through MGS aerobraking and the MCD outputs was 0.321, as shown in Figure 5.

Mars Odyssey aerobraking measured the northern high-latitude 130-km neutral densities at Ls 263°–304° in MY25. As discussed in Section 2, because the ODY perigee height was far lower than 130 km during this period, the inbound and outbound observations were considerably different in latitudes, local times, and SZAs. Therefore, the inbound and outbound observations were com-

pared separately with the MCD v4.3 outputs. Additionally, the ODY aerobraking data were 5-point running averaged.

Figure 6 shows the comparison between the ODY aerobraking observations and the MCD simulation results. The outbound data are plotted in Figure 6a, and the inbound data in Figure 6b. The blue diamonds represent aerobraking observations, the red dots represent uncorrected MCD v4.3 outputs, the red asterisks represent corrected MCD v4.3 outputs, and the black crosses represent uncorrected MCD v4.3 outputs with a negative shift of about  $3 \times 10^{10} \text{cm}^{-3}$ , which mostly agree with the ODY observations after Ls 290°. In Figure 6, we can see fluctuations and bursts in the ODY-observed neutral densities at 130 km similar to those in the MGS aerobraking observations. For the outbound observations, the corrected MCD v4.3 outputs were quite consistent with observations after Ls 295°, but the former were larger than the latter when Ls < 290°. Similar phenomena are also shown in the MGS observations in Figure 5. These phenomena may be related to deficiencies in MCD v4.3, as discussed in Section 5. For the inbound observations, the corrected MCD v4.3 outputs were still somewhat larger than the observations. After subtracting  $3 \times 10^{10} \text{cm}^{-3}$  from the uncorrected MCD outputs, the MCD results basically agreed with the ODY observations after Ls 290°. We believe that the mismatch between the corrected MCD outputs and the ODY inbound observations may have been caused by both an ODY aerobraking observational error and some deficiencies in MCD v4.3, as discussed in the next section. The correlation coefficient between the ODY aerobraking-observed densities and the MCD outputs for the outbound data was 0.568, and that for the inbound data was 0.536.

As can be seen, the correlation coefficients between the MCD outputs and aerobraking observations for the ODY/accelerometer (ACC) and MGS/ACC (0.321, 0.568, and 0.536, respectively) were much lower than those for the MGS/radio occultation (RO; 0.886, 0.909, and 0.817). Except for the differences in observational errors and seasons (as discussed in Section 5), one main reason for the low correlation coefficients may be the shorter observational durations in the cases of MGS/ACC and ODY/ACC.

Generally, the MCD is more suitable for simulating or forecasting the long-term and large-scope averaged variations of Martian

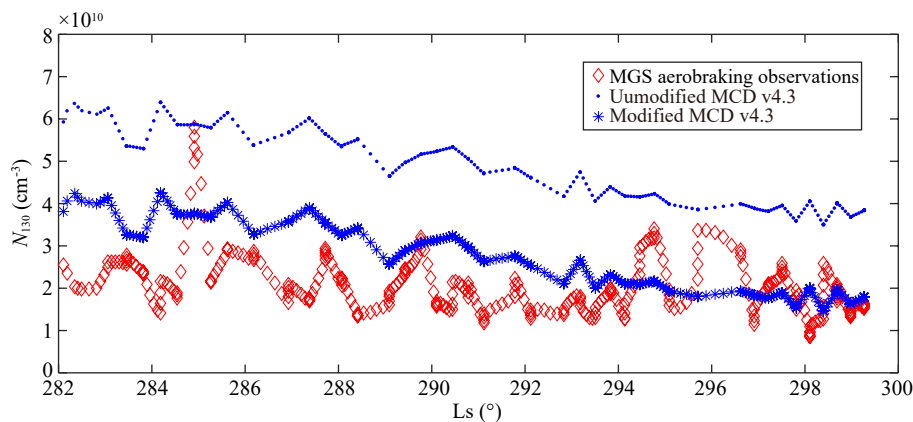


**Figure 5.** MGS aerobraking-observed 130-km neutral densities (red diamonds), unmodified MCD v4.3 simulations (blue dots), and modified MCD v4.3 simulations (blue asterisks).

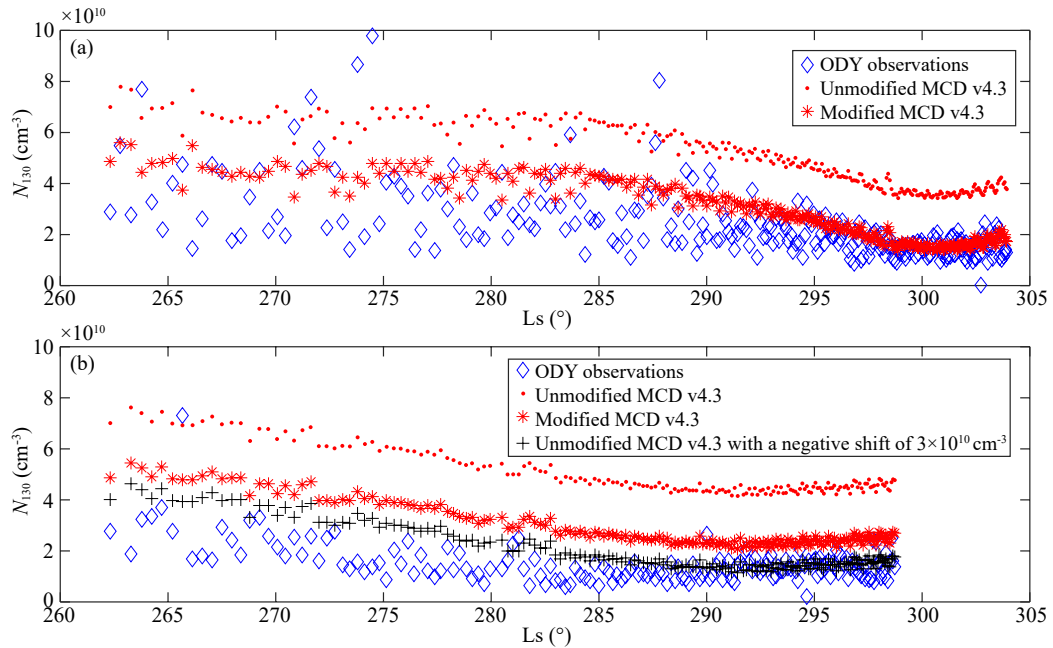


**Figure 6.** (a) ODY aerobraking outbound observations (blue diamonds), uncorrected MCD v4.3 outbound results (red dots), and corrected MCD v4.3 outbound results (red asterisks); (b) ODY aerobraking inbound observations (blue diamonds), uncorrected MCD v4.3 inbound results (red dots), corrected MCD v4.3 inbound results (red asterisks), and uncorrected MCD v4.3 inbound outputs with the shift of  $-3 \times 10^{10} \text{cm}^{-3}$  (black crosses).

neutral densities, such as those caused by seasonal variations, latitude variations, and global dust storms. To date, simulations of the atmospheric waves have caused variations and short-term, local dust storms have caused variations in the Martian neutral densities that are still not clear; in addition, a series of interpolation processes were used when generating the MCD outputs, all making the MCD unsuitable for simulating short-term, local variations in the neutral densities (Millour et al., 2008).

In our case, all the durations of the MGS/RO observations were longer than  $100^{\circ} L_s$ , whereas the durations of the MGS/ACC observations were only about  $19^{\circ} L_s$  and those of the ODY/ACC observations were shorter than  $40^{\circ} L_s$ . Because of the existence of short-term, local neutral density variations, which cannot be simulated well by the MCD, as well as observational errors, the longer the observational duration, the greater would be the proportion of long-term neutral density variations in the total variations and the higher the correlation coefficient would be. Some of the short-term, local variations of accelerometer-observed neutral densities could be removed by the running average process. When the 5-point running average was calculated, the correlation coefficients for MGS/ACC and ODY/ACC increased to 0.502 (for MGS/ACC), 0.840 (for ODY/ACC outbound), and 0.766 (for ODY/ACC inbound).

## 5. Discussion

The upper atmosphere of Mars is quite unstable. Variations in solar radiation, dust storm activities, strength of the atmospheric circulation, and waves in the lower atmosphere can all significantly affect the densities of the Martian upper atmosphere, resulting in density variations at different seasons, latitudes, longitudes, and local times. In the dust storm season, modeling the Martian upper

atmospheric densities will be more difficult because of the frequent dust storm activity and consequent variations in the strength of atmospheric circulation (Conrath et al., 2000; Lewis et al., 2007; Medvedev et al., 2013). From the above comparison between aerobraking observations of the MGS and ODY and the modified MCD v4.3 outputs, we found deficiencies in MCD v4.3 when simulating Martian northern high-latitude atmospheric densities at 130 km during the dust storm seasons.

Because the MGS/RO observations took place mainly in the non-dust-storm seasons, the calculated 130-km neutral densities were consistent with the modified MCD v4.3 outputs in nearly all the observation periods. The only exception ( $L_s 135^{\circ}$ – $145^{\circ}$ , MY27) was due to local dust storm activity, as reported by Qin JF et al. (2019a). These local dust storms caused variations in the upper atmospheric densities that could not be simulated well by the MCD (Millour et al., 2008), causing the correlation coefficient between MCD and MGS/RO observations in MY27 (0.817) to be slightly lower than those in MY25 and MY26 (0.886 and 0.909, respectively). Similarly, the frequent occurrence of local, short-term dust storms in the dust storm seasons was implicated in the large, sudden increases in the MGS/ACC- and ODY/ACC-observed neutral densities, which is likely one reason for the lower correlation coefficients in the accelerometer observations (0.321, 0.568, and 0.536) compared with the MGS/RO observations. As shown in Figures 5 and 6, both MGS and ODY aerobraking registered neutral densities at 130 km that were considerably lower than the modified MCD v4.3 outputs before  $L_s 295^{\circ}$ . During dust storm seasons, the upper atmospheric densities are mainly controlled by global dust storm activities, which can be quantified by the global average atmospheric opacity. Because observations before MY24 were lacking, only the atmospheric opacity data in MY24

and in the period during ODY aerobraking observations could be derived (Montabone et al., 2015). As shown in Figure 7, the global average atmospheric opacities in MY25 were universally higher than in MY24 during Ls 260°–300°. When the atmospheric opacity is elevated, the low and middle atmosphere will become heated and extend more dramatically, and the upper atmospheric densities will then become higher. However, the ODY aerobraking-observed densities in MY25 were lower than the modified MCD v4.3 outputs, which were based on MY24 dust scenarios. This means that MCD v4.3 tended to overestimate the effect of dust storms on the northern high-latitude neutral densities at 130 km.

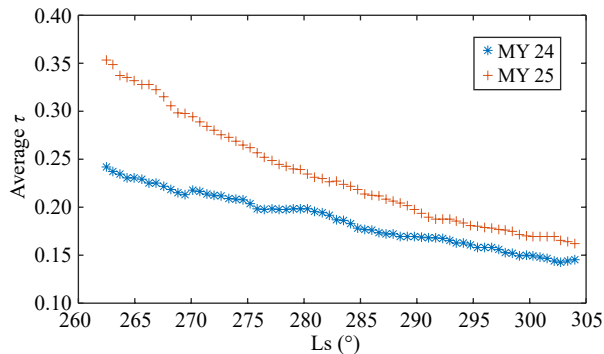


**Figure 7.** Global average atmospheric opacities in MY24 and MY25 during Ls 262–304°.

Because the ODY aerobraking inbound and outbound observations had different latitudes and local times, comparison between the ODY observations and the modified MCD v4.3 outputs allowed us to analyze the performance of MCD v4.3 in simulating northern high-latitude 130-km neutral densities at different latitudes and local times. These data sets are displayed in Figure 8. Figure 8a shows ODY observations of 130-km neutral densities, and Figure 8b shows unmodified MCD v4.3 outputs. Figure 8c and 8d show latitudes and local times. The blue symbols represent inbound observations, and the red symbols represent outbound observations.

Intuitively, we can see from Figure 8a that the variations of the outbound observations are considerably larger than those of the inbound observations before Ls 290°. As mentioned, these sudden increases (such as Ls 270°–275° and Ls 287°–290°) may be the effects of local or short-term dust storms. The difference between inbound and outbound observations of these sudden, dust-storm-caused disturbances can be related to the latitude variations. As shown in Figure 8c, when Ls < 290°, the outbound observations (red symbols) were mainly made at 60°–70°N, whereas the inbound observations (blue symbols) were all made above 75°N. According to previous research, Martian dust storms can significantly increase the strength of atmospheric circulation and can then affect the atmospheric temperature and density at high latitudes by enhancing the atmospheric adiabatic sinking movement in the polar regions. At Ls ~270°, the subsolar point was south of the Martian equator. Therefore, the latitude where the northern branch of the circulation airflow sank could not be as high as 80°N. Because of this, in the outbound observations, the neutral densities at 130 km were easily affected by dust storm activities,

but in the inbound observations, the neutral densities at 130 km were much less affected. After Ls 290°, both the inbound and outbound observations of the 130-km neutral densities became stable, even though at that time, the inbound observations were made at 60°–70°N. This can be explained by the decline in global dust storm activities (see Figure 7). At Ls ~293°, both the inbound and outbound observations were taken in the latitude around 75°N, but the outbound observations were made at a local time of about 16:00, whereas the inbound observations were made at a local time of about 04:00. The difference in local time caused the 130-km neutral atmospheric densities from the outbound observations to be about  $10^{10}\text{cm}^{-3}$  greater than the densities from the inbound observations. This is because in the dayside, the Martian atmosphere is heated and expands, whereas in the nightside, the Martian atmosphere cools down so that the 130-km neutral densities at 16:00 are greater than those at 04:00.

From our comparison between the ODY observations and the MCD v4.3 outputs, we believe that the simulations of MCD v4.3 tended to underestimate the effect of latitude variations on the 130-km neutral densities under high dust storm activities and to overestimate the effect under low dust storm activities. As shown in Figure 8, before Ls 275°, the local time difference of the inbound and outbound observations was small but the difference in latitude was quite large. As mentioned above, during this period, the ODY observations showed great diversity between the 130-km neutral densities of the lower-latitude regions (outbound data with latitudes of 60°–70°N) and the high-latitude regions (inbound data with latitudes of > 75°N). However, the inbound and outbound densities simulated by MCD v4.3 were very close to each other before Ls 275°. From this fact, it can be speculated that the effect of the sinking airflow on 130-km neutral densities was underestimated by MCD v4.3, so the northern high-latitude 130-km neutral density variations at different latitudes under high dust storm activities were not evident in the MCD v4.3 outputs. During Ls 275°–290°, the differences between inbound and outbound densities simulated by MCD v4.3 were basically consistent with those observed by ODY aerobraking. These differences in 130-km densities are more relevant to the disparity between local times than to the latitudes. As shown in Figure 8b, when Ls > 290°, the MCD v4.3 outputs were highly dependent on the variations in latitude for both the inbound and outbound observations, with higher densities at lower latitudes. However, the ODY-observed 130-km neutral densities in this period were very stable and not as dependent as the MCD outputs on latitude variations. This result means that under low dust storm activities, the MCD v4.3 outputs tended to overestimate the effect of latitude variations on northern high-latitude 130-km neutral densities. We can also see that at Ls ~293°, the difference between the inbound and outbound densities simulated by MCD v4.3 agreed with those observed by ODY, meaning that MCD v4.3 was able to correctly estimate the effect of local time variations on the northern high-latitude neutral densities at 130 km.

As shown in Figure 6, a remaining problem is that the modified MCD v4.3 outputs were still higher than the ODY-observed inbound densities. However, we can now link this mismatch to the previous analysis of the MGS and ODY aerobraking observations

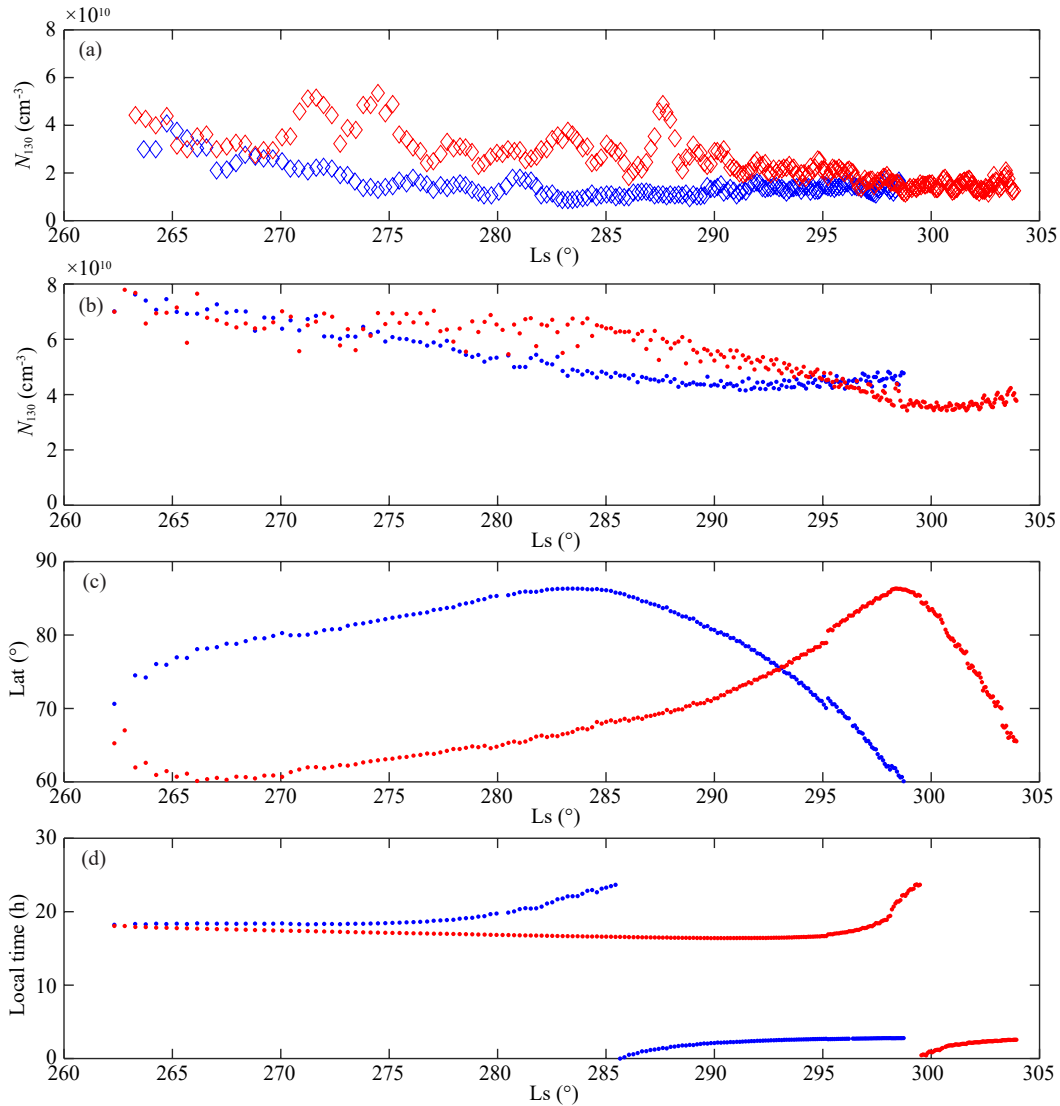


**Figure 8.** (a) ODY aerobraking-observed 130-km neutral densities (blue: inbound observations; red: outbound observations); (b) MCD v4.3 simulated 130-km neutral densities (blue: inbound observations; red: outbound observations); (c, d) the latitude and local time of ODY observations (blue: inbound observations; red: outbound observations).

and the MCD v4.3 outputs above. The effects of underestimating the latitude on 130-km neutral densities before Ls 290° and of overestimating the latitude after Ls 290° would both result in larger than expected inbound outputs from MCD v4.3 during Ls 260°–300° so that even after modification, the MCD v4.3 outputs would still be larger than the ODY inbound observations. Apart from this interior defect of MCD v4.3, the systematic error in ODY aerobraking measurements, as mentioned in Section 2.2, may also play a part in this mismatch.

In general, the variations in Martian northern high-latitude neutral densities at 130 km are quite complex and are controlled by many factors during the dust storm seasons. The models used to simulate the upper atmosphere during this period need to be further optimized, and relevant observation data need to be further enriched. Nevertheless, we consider the 130-km neutral densities calculated from the MGS radio occultation experiments credible enough to help calibrate and improve future Martian atmosphere models.

## 6. Conclusions

In this study, coupling between the ionosphere and neutral atmosphere was used to derive the neutral atmospheric densities at 130 km in the high-latitude region of the Martian northern hemisphere from electron density profiles measured by the MGS Radio Science Experiment. The calculated density data were compared with the neutral densities simulated by MCD v4.3 and those measured by aerobraking observations of the MGS and ODY.

We found that the calculated 130-km neutral atmospheric densities based on MGS occultation observations were in good agreement with the MCD v4.3 simulations after modifying the MCD outputs (i.e., after subtracting  $2 \times 10^{10} \text{cm}^{-3}$  from the original outputs). This modification still worked in adjusting the MCD v4.3 simulations for consistency with the MGS and ODY aerobraking observations. When the modified MCD v4.3 simulations were compared with the MGS and ODY aerobraking observations, we found that MCD v4.3 tended to overestimate the effects of the

dust storm activities and underestimate the effects of latitude variations on the 130-km neutral densities at northern high latitudes when the dust storms activities were frequent, and that it tended to overestimate the effects of latitude variations on the 130-km neutral densities at northern high latitudes when the dust storm activities declined.

This research illustrates that the method used to calculate 130-km neutral densities through ionospheric profiles was effective and that the technique used to modify the MCD v4.3 outputs was reasonable. The MCD v4.3 simulations of the high-latitude upper atmosphere in dust storm seasons still need to be improved further; however, the calculated 130-km neutral densities from MGS radio occultation measurements are trustworthy for calibrating current and future atmosphere models of Mars.

## Acknowledgments

We thank the MGS Radio Science Team, the MGS Aerobraking Team, and the ODY Aerobraking Team for uploading their excellent ionospheric and neutral atmospheric data to their website. We thank the LMD group in Paris for providing the MCD data. This research was funded by the National Science Foundation of China (NSFC, no. 41674175) and was also supported by the preresearch Project on Civil Aerospace Technologies (no. D020105) funded by the China National Space Administration.

## References

- Bougher, S. W., Keating, G. M., Forbes, J. M., Murphy, J. R., Hollingsworth, J. L., Wilson, R. J., and Withers, P. G. (2001). The upper atmospheric wave structure of Mars as determined by Mars Global Surveyor. In *AGU Fall Meeting Abstracts*. San Francisco, California: AGU.
- Bougher, S. W., Pawlowski, D., Bell, J. M., Nelli, S., McDunn, T., Murphy, J. R., Chizek, M., and Ridley, A. (2015). Mars global ionosphere-thermosphere model: solar cycle, seasonal, and diurnal variations of the Mars upper atmosphere. *J. Geophys. Res. Planets*, *120*(2), 311–342. <https://doi.org/10.1002/2014JE004715>
- Breus, T. K., Krymskii, A. M., Crider, D. H., Ness, N. F., Hinson, D., and Barashyan, K. K. (2004). Effect of the solar radiation in the topside atmosphere/ionosphere of Mars: Mars Global Surveyor observations. *J. Geophys. Res. Space Phys.*, *109*(A9), A09310. <https://doi.org/10.1029/2004JA010431>
- Clancy, R. T., and Lee, S. W. (1991). A new look at dust and clouds in the Mars atmosphere: analysis of emission-phase-function sequences from global Viking IRTM observations. *Icarus*, *93*(1), 135–158. [https://doi.org/10.1016/0019-1035\(91\)90169-T](https://doi.org/10.1016/0019-1035(91)90169-T)
- Conrath, B. J., Pearl, J. C., Smith, M. D., Maguire, W. C., Christensen, P. R., Dason, S., and Kaelberer, M. S. (2000). Mars Global Surveyor Thermal Emission Spectrometer (TES) observations: Atmospheric temperatures during aerobraking and science phasing. *J. Geophys. Res. Planets*, *105*(E4), 9509–9519. <https://doi.org/10.1029/1999JE001095>
- Dong, C. F., Bougher, S. W., Ma, Y. J., Toth, G., Curry, S. M., Nagy, A. F., Halekas, J. S., Luhmann, J. G., Mahaffy, P., ... Jakosky, B. M. (2015). Solar wind Mars interaction during the MAVEN Deep Dip campaigns: multi-fluid MHD simulations based upon the SWIA, NGIMS and MAG measurements. In *American Astronomical Society, DPS Meeting #47*. National Harbor, Maryland: AAS.
- Fjeldbo, G., Fjeldbo, W. C., and Eshleman, V. R. (1966). Models for the atmosphere of Mars based on the Mariner 4 occultation experiment. *J. Geophys. Res.*, *71*(9), 2307–2316. <https://doi.org/10.1029/JZ071i009p02307>
- Forget, F., Bibring, J. P., Bertaux, J. L., Formisano, V., Paetzold, M., Coll, M. A. I., Bottger, H., Douté, S., Drossart, P., ... Schmitt, B. (2009). Analysis of the Mars Express observations of the atmosphere and the polar caps: interpretation with a global climate model. In *First Mars Express Science Conference*. Noordwijk, Netherlands: ESA/ESTEC.
- Fritts, D. C., Wang, L., and Tolson, R. H. (2006). Mean and gravity wave structures and variability in the Mars upper atmosphere inferred from Mars Global Surveyor and Mars Odyssey aerobraking densities. *J. Geophys. Res. Space Phys.*, *111*(A12), A12304. <https://doi.org/10.1029/2006JA011897>
- González-Galindo, F., Bougher, S., López-Valverde, M. A., Forget, F., and Bell, J. (2006). Thermal structure of the Martian thermosphere: LMD-IAA GCM and MTGCM intercomparisons. In F. Forget, et al. (Eds.), *Mars Atmosphere Modelling and Observations*. Granada, Spain: LMD, IAA, AOPP, CNES, ESA.
- Gröller, H., Yelle, R. V., Montmessin, F., Lacombe, G., Schneider, N. M., Stewart, I., Deighan, J., McClintock, W. E., Clarke, J. T., ... Jakosky, B. M. (2015). Martian CO<sub>2</sub> and O<sub>2</sub> abundances obtained from MAVEN/IUVS stellar occultations. In *European Planetary Science Congress*. Nantes, France.
- Herschel, W. (1784). On the remarkable appearances at the polar regions of the planet Mars, and its spheroidal figure; with a few hints relating to its real diameter and atmosphere. *Phil. Trans.*, *74*, 233–273. <https://doi.org/10.1098/rstl.1784.0020>
- Hinson, D. P., Simpson, R. A., Twicken, J. D., Tyler, G. L., and Flasar, F. M. (1999). Initial results from radio occultation measurements with Mars Global Surveyor. *J. Geophys. Res. Planets*, *104*(E11), 26997–27012. <https://doi.org/10.1029/1999JE001069>
- Hinson, D. P., Smith, M. D., and Conrath, B. J. (2004). Comparison of atmospheric temperatures obtained through infrared sounding and radio occultation by Mars Global Surveyor. *J. Geophys. Res. Planets*, *109*(E12), E12002. <https://doi.org/10.1029/2004JE002344>
- Jain, S., Stewart, I., Schneider, N. M., Deighan, J., Stiepen, A., Evans, J. S., Stevens, M. H., Chaffin, M. S., Crismani, M., ... Jakosky, B. (2016). Martian upper atmosphere response to solar EUV flux and soft X-ray flares. AAS/division for Planetary Sciences Meeting. In *AAS/Division for Planetary Sciences Meeting Abstracts #48*. Pasadena, California.
- Jakosky, B. M., and Farmer, C. B. (1982). The seasonal and global behavior of water vapor in the Mars atmosphere: complete global results of the Viking atmospheric water detector experiment. *J. Geophys. Res. Solid Earth*, *87*(B4), 2999–3019. <https://doi.org/10.1029/JB087iB04p02999>
- Keating, G. M., Theriot, M. Jr., Tolson, R., Bougher, S., Forget, F., and Forbes, J. (2003). Global measurements of the Mars upper atmosphere: In situ accelerometer measurements from Mars Odyssey 2001 and Mars Global Surveyor. In *Proceedings of the 34th Annual Lunar and Planetary Science Conference*. League City, Texas.
- Keating, G. M., Bougher, S. W., Theriot, M. E., Tolson, R. H., Zurek, R. W., Blanchard, R. C., Murphy, J. R., and Bertaux, J. L. (2007). Mars neutral upper atmosphere temporal and spatial variations discovered from the accelerometer science experiment aboard Mars reconnaissance orbiter. In *Proceedings of the 38th Lunar and Planetary Science Conference, (Lunar and Planetary Science XXXVIII)* (pp. 2074). League City, Texas: LPI.
- Keating, J. M., Bougher, S. W., Zurek, R. W., Tolson, R. H., Cancro, G. J., Noll, S. N., Parker, J. S., Schellenberg, T. J., Shane, R. W., ... Babicke, J. M. (1998). The structure of the upper atmosphere of Mars: In situ accelerometer measurements from Mars Global Surveyor. *Science*, *279*(5357), 1672–1676. <https://doi.org/10.1126/science.279.5357.1672>
- Kleinböhl, A., Schofield, J. T., Kass, D. W., Abdou, W. A., Backus, C. R., Sen, B., Shirley, J. H., Lawson, W. G., Richardson, M. I., ... McCreese, D. J. (2009). Mars Climate Sounder limb profile retrieval of atmospheric temperature, pressure, and dust and water ice opacity. *J. Geophys. Res. Planets*, *114*(E10), E10006. <https://doi.org/10.1029/2009JE003358>
- Lewis, S. R., Read, P. L., Conrath, B. J., Pearl, J. C., and Smith, M. D. (2007). Assimilation of thermal emission spectrometer atmospheric data during the Mars Global Surveyor aerobraking period. *Icarus*, *192*(2), 327–347. <https://doi.org/10.1016/j.icarus.2007.08.009>
- Mahaffy, P. R., Benna, M., Elrod, M., Yelle, R. V., Bougher, S. W., Stone, S. W., and Jakosky, B. M. (2015). Structure and composition of the neutral upper atmosphere of Mars from the MAVEN NGIMS investigation. *Geophys. Res. Lett.*, *42*(21), 8951–8957. <https://doi.org/10.1002/2015GL065329>
- Medvedev, A. S., Yiğit, E., Kuroda, T., and Hartogh, P. (2013). General circulation

- modeling of the Martian upper atmosphere during global dust storms. *J. Geophys. Res. Planets*, 118(10), 2234–2246. <https://doi.org/10.1002/2013JE004429>
- Millour, E., Forget, F., González-Galindo, F., Spiga, A., Lebonnois, S., Montabone, L., Lewis, S. R., Read, P. L., López-Valverde, M. A., ... Huot, J. P. (2008). The latest (version 4.3) Mars climate database. In *Third International Workshop on The Mars Atmosphere: Modeling and Observations*. Williamsburg, Virginia: LPI.
- Montabone, L., Forget, F., Millour, E., Wilson, R. J., Lewis, S. R., Cantor, B., Kass, D., Kleinböhl, A., Lemmon, M. T., ... Wolff, M. J. (2015). Eight-year climatology of dust optical depth on Mars. *Icarus*, 251, 65–95. <https://doi.org/10.1016/j.icarus.2014.12.034>
- Nier, A. O., and McElroy, M. B. (1976). Structure of the neutral upper atmosphere of Mars: results from Viking 1 and Viking 2. *Science*, 194(4271), 1298–1300. <https://doi.org/10.1126/science.194.4271.1298>
- Qin, J. F., Zou, H., Ye, Y. G., Yin, Z. F., Wang, J. S., and Nielsen, E. (2019a). Effects of local dust storms on the upper atmosphere of Mars: Observations and simulations. *J. Geophys. Res. Planets*, 124(2), 602–616. <https://doi.org/10.1029/2018JE005864>
- Qin, J. F., Zou, H., and Ye, Y. G. (2019b). Study of Mars' upper atmosphere based on radio occultation observations. *Spacecr. Environ. Eng. (in Chinese)*, 36(6), 571–583.
- Ryan, J. A. (1985). Mars atmospheric circulation: aspects from Viking landers. *J. Geophys. Res. Space Phys.*, 90(A7), 6319–6325. <https://doi.org/10.1029/JA090iA07p06319>
- Tolson, R. H., Keating, G. M., Cancro, G. J., Parker, J. S., Noll, S. N., and Wilkerson, B. L. (1999). Application of accelerometer data to Mars global surveyor aerobraking operations. *J. Spacecr. Rockets*, 36(3), 323–329. <https://doi.org/10.2514/2.3474>
- Tolson, R. H., Dwyer, A. M., Hanna, J. L., Keating, G. M., George, B. E., Escalera, P. E., and Werner, M. R. (2005). Application of accelerometer data to Mars odyssey aerobraking and atmospheric modeling. *J. Spacecr. Rockets*, 42(3), 435–443. <https://doi.org/10.2514/1.15173>
- Wang, J. S. and Nielsen, E. (2013). Behavior of the Martian dayside electron density peak during global dust storms. *Planetary and Space Science*, 51(4–5), 329–338. [https://doi.org/10.1016/S0032-0633\(03\)00015-1](https://doi.org/10.1016/S0032-0633(03)00015-1)
- Wilson, R. J. (2002). Evidence for nonmigrating thermal tides in the Mars upper atmosphere from the Mars global surveyor accelerometer experiment. *Geophys. Res. Lett.*, 29(7), 24-1–24-4. <https://doi.org/10.1029/2001GL013975>
- Withers, P. and Pratt, R. (2013). An observational study of the response of the upper atmosphere of Mars to lower atmospheric dust storms. *Icarus*, 225(1), 378–389. <https://doi.org/10.1016/j.icarus.2013.02.032>
- Zhang, M. H. G., Luhmann, J. G., Kliore, A. J., and Kim, J. (1990). A post- Pioneer Venus reassessment of the Martian dayside ionosphere as observed by radio occultation methods. *J. Geophys. Res. Solid Earth*, 95(B9), 14829–1483. <https://doi.org/10.1029/JB095iB09p14829>
- Zou, H., Wang, J. S., and Nielsen, E. (2005). Effect of the seasonal variations in the lower atmosphere on the altitude of the ionospheric main peak at Mars. *J. Geophys. Res. Space Phys.*, 110(A9), A09311. <https://doi.org/10.1029/2004JA010963>
- Zou, H., Wang, J. S., and Nielsen, E. (2006). Reevaluating the relationship between the Martian ionospheric peak density and the solar radiation. *J. Geophys. Res. Space Phys.*, 111(A7), A07305. <https://doi.org/10.1029/2005JA011580>
- Zou, H., Lillis, R. J., Wang, J. S., and Nielsen, E. (2011). Determination of seasonal variations in the Martian neutral atmosphere from observations of ionospheric peak height. *J. Geophys. Res. Planets*, 116(E9), E09004. <https://doi.org/10.1029/2011JE003833>
- Zou, H., Ye, Y. G., Wang, J. S., Nielsen, E., Cui, J., and Wang, X. D. (2016). A method to estimate the neutral atmospheric density near the ionospheric main peak of Mars. *J. Geophys. Res. Space Phys.*, 121(4), 3464–3475. <https://doi.org/10.1002/2015JA022304>
- Zurek, R. W. (2017). Understanding Mars and its atmosphere. In R. M. Haberle, et al. (Eds.), *The Atmosphere and Climate of Mars* (pp. 3–19). Cambridge: Cambridge University Press.